Grid resolution effects on LES of a piloted methane-air flame

K. A. Kemenov[*], H. Wang, S. B. Pope

Sibley School of Mechanical and Aerospace Engineering,
Cornell University, Ithaca, NY 14853

Abstract

The grid dependence of LES of a piloted methane-air (Sandia D) flame is studied on a series of grids with progressively increased resolution reaching about 10 million cells. Chemical compositions, density and temperature fields are modeled based on the evolution of mixture fraction combined with a steady flamelet model. However, to minimize interpolation uncertainties that are routinely introduced by a standard flamelet look-up table procedure, we adopt a simple smooth analytical relationship for specific volume and temperature as functions of mixture fraction. Such an analytical relationship can be easily inferred by approximating a steady flamelet solution by quadratic functions that are known to give a quite accurate representations of the lean mixtures. The simulation results are discussed and compared with available experimental data. In particular, the dependence of LES turbulent statistics on the turbulence resolution length scale is analyzed and tested for the existence of intermediate inertial range asymptotic behavior. For the most part, the statistics converge for the finest grids, but the RMS of the mixture fraction early in the flame shows some residual grid dependence.

Introduction

Large Eddy Simulation (LES) has proved to be an effective simulation approach for a wide range of turbulent flows including chemically reactive turbulent flows [1, 2, 3, 4]. This latter class of flows adds an extra set of challenges to LES modeling. In addition to accounting for the effects of the unresolved dynamic scales, the small-scale molecular mixing and chemical reaction processes, which usually occur on scales much smaller than LES grid, have to be modeled as well. Nevertheless, the number of successful applications of LES accompanied by rather sophisticated combustion models [5, 6, 7, 8, 9], as well as by models with simplified chemistry treatment, [10, 11, 12, 13] has been growing, and these simulations have demonstrated the attractiveness of the approach not only for canonical geometries like laboratory jet flames but also for complex ones like gas-turbine combustors [14, 15, 16].

In this work we focus on one of the canonical flame configuration from the TNF flame series – Sandia flame D. This piloted non-premixed methane-air flame has been extensively studied experimentally by Barlow & Frank [17] and by Schneider et al. [18], and, as a result, it represents an ideal benchmark case for testing and developing combustion models in the context of LES. A number of LES studies of Sandia flame D have been performed successfully in the past [11, 19, 20, 13, 21] with combustion models of varying complexity. Most combustion models center on a mixture fraction based flamelet approach [22], where chemical composition, temperature and density are parametrized by one (or a few) field variables such as the mixture fraction $\xi(\boldsymbol{x}, t)$ and its scalar dissipation rate, or a specially constructed progress variable [23]. Such a parametrization produces a flamelet table which represents a discrete approximation of a smooth surface (manifold) in the space of thermochemical variables so that all chemical species, temperature and density can be retrieved from the flamelet table if values of the parametrized variables are provided. The predictive accuracy, thus, is based on two things: (i) the parametrizing variables, i.e., the mixture fraction (and others variables) should be accurately predicted from integration of their LES evolution equations; and (ii), the flamelet parametrization should adequately approximate the chemical reaction manifold. While such a simplified turbulence/chemistry interaction treatment might fall short in representing realistic combustion chemistry, as opposed to more advanced and technically elaborated approaches such as transported PDF based methods [24, 20], it provides a useful tool to study particular effects of sub-filter scale or/and combustion models on the LES solution.

Here, we follow a similar simplified approach by representing the chemistry by a single mildly-strained steady flamelet solution based on integration of a one-dimensional counter-flow diffusion flame with the detailed GRI-Mech 3.0 chemical mechanism. A flamelet solution is obtained from the OPPDIF module of the CHEMKIN commercial software. Instead of forming a flamelet table, we approximate the flamelet solution for specific volume and temperature by quadratic functions of the mixture fraction, i.e., $\rho^{-1}(\xi) = a + b\xi + c\xi^2$ and $T(\xi) = a_T + b_T\xi + c_T\xi^2$. These approximations are smooth, and hence eliminate flamelet table interpolation uncertainties, and provide an accurate fit to the flamelet solution for lean mixtures, while slightly underpredicting density and overpredicting temperature for rich mixtures correspondingly. Mixture transport properties, such as molecular viscosity and diffusivity, are also obtained from the flamelet solution and are fitted to a power law form in temperature, before being used in the LES equations.

---

[*]Corresponding author: kak262@cornell.edu

LES focuses on the explicit simulation of the large (resolved) scales of the turbulent motion where the effect of unresolved scales is represented by a model. The resolved LES field $\mathbf{u}^L(\mathbf{x}, t)$ is very often associated with spatial filtering of the underlying turbulent field, resulting in the filtered field $\overline{\mathbf{u}}(\mathbf{x}, t)$. While such a definition of the resolved fields can be somewhat helpful in derivation of the LES equations, albeit under very restrictive conditions of the uniformity of filter width and commutativity between filtering and differentiation, generally it appears to be misleading as discussed, for example, in [25]. The resolved LES field is defined as the solution of the LES equations. We further note that invoking the concept of filtering in deriving LES equations is at least debatable since these equations arise naturally in multiscale formulations [26], or in regularization of the Navier-Stokes equations [27] without making use of filters. The LES solution depends on the filter width $\Delta(\mathbf{x})$, or more appropriately, on the turbulence resolution length scale [25], as it explicitly enters models for the SGS stress.

Following [25], let Q^m and Q denote statistics of interest that are derived from an LES solution and from the full turbulent field, respectively. For example, these can be mean values of the resolved and full mixture fractions, i.e., $Q^m = \langle \xi^L(\mathbf{x}, t) \rangle$ and $Q = \langle \xi(\mathbf{x}, t) \rangle$. In practice, the predictive capabilities of LES are judged based on comparison of LES statistics Q^m to the "true" statistics Q obtained from the high-resolution experiments or, for low Re-number flows, from DNS. However, as was discussed by Pope [25], a comparison based on a single LES realization cannot be deemed satisfactory, since LES statistics depend on the turbulence resolution scale $\Delta(\mathbf{x})$. Therefore, to evaluate the fidelity of LES predictions it is necessary to consider the dependence of LES statistics on $\Delta(\mathbf{x})$, i.e., $Q^m(\Delta(\mathbf{x}))$. Furthermore, based on such dependence, several criteria on how to compare different LES models with respect to accuracy and cost can be formulated [25]. These criteria use a notion of the intermediate statistic asymptote Q_I^m that represents values of LES statistics which are, in a certain resolution range, independent of $\Delta(\mathbf{x})$. A study of the sensitivity of LES statistics to $\Delta(\mathbf{x})$ gains more relevance for LES of combustion systems. In turbulent combustion, the rate controlling processes such as reactant mixing and chemical reactions occur on the small scales which are usually much smaller than $\Delta(\mathbf{x})$. As a result, the resolved effect of the complex small-scale turbulence/chemistry interactions is modeled in an affordable way by a combustion model. A question of how a particular combustion model affects LES statistics with respect to the true statistics Q can be studied based on $Q^m(\Delta(\mathbf{x}))$.

In this work we apply a simple combustion model to study the effects of $\Delta(\mathbf{x})$, i.e., resolution effects, on statistics of the mixture fraction $\xi^L(\mathbf{x}, t)$ and velocity $\mathbf{u}^L(\mathbf{x}, t)$ fields in LES of Sandia flame D. Mean and root mean square (RMS) values are chosen to be representative statistics since corre-

sponding experimental data are readily available for comparison [17, 18]. We focus mainly on the mixture fraction because of its importance in non-premixed combustion modeling. Many flamelet-based approaches involve the mixture fraction which is used to parametrize chemical composition, molecular properties and enthalpy. And therefore, it is a minimal requirement to accurately predict an evolution of the mixture fraction.

Specific Objectives

In LES of variable-density turbulent flows with parametrized chemistry one solves large-scale evolution equations for the resolved density, and the density weighted velocity and the mixture fraction fields. With a little abuse of notation, they are customary denoted as $\bar{\rho}$, $\tilde{u}_i$ and $\tilde{\xi}$, respectively. Here, the common Favre notation for the density weighted resolved quantity is used, i.e., $\tilde{\xi} = \overline{\rho \xi}/\bar{\rho}$. The combustion model is specified through quadratic relationships between specific volume and temperature which results in the following resolved equations:

$$1/\bar{\rho} = \widetilde{1/\rho} = a + b\tilde{\xi} + c\widetilde{\xi^2}, \quad \widetilde{T} = a_T + b_T\tilde{\xi} + c_T\widetilde{\xi^2} \quad (1)$$

These relationships are nonlinear and depend on the subgrid scale fluctuations of the mixture fraction which are usually characterized by the subgrid scale variance $V_\xi = \widetilde{\xi^2} - \tilde{\xi}^2$. Instead of solving a transport equation for V_ξ directly, in this work we carry an equation for $\widetilde{\xi^2}$ explicitly. This proves to be more advantageous since the latter equation does not contain extra production terms [8]. Thus, the considered LES system of the governing equations is given by:

$$\frac{\partial \bar{\rho}}{\partial t} + \frac{\partial \overline{\rho}\widetilde{u}_j}{\partial x_j} = 0, \quad (2)$$

$$\frac{\partial \bar{\rho}\widetilde{u}_i}{\partial t} + \frac{\partial \bar{\rho}\widetilde{u}_i\widetilde{u}_j}{\partial x_j} = -\frac{\partial \bar{p}}{\partial x_i} + 2\frac{\partial}{\partial x_j}\Big((\bar{\mu} + \mu_T)(\widetilde{S}_{ij} - \quad (3)$$

$$-\frac{1}{3}\widetilde{S}_{kk}\delta_{ij})\Big),$$

$$\frac{\partial \bar{\rho}\tilde{\xi}}{\partial t} + \frac{\partial \bar{\rho}\widetilde{u}_j\tilde{\xi}}{\partial x_j} = \frac{\partial}{\partial x_j}\Big(\bar{\rho}(\widetilde{D} + D_T)\frac{\partial\tilde{\xi}}{\partial x_j}\Big), \quad (4)$$

$$\frac{\partial \bar{\rho}\widetilde{\xi^2}}{\partial t} + \frac{\partial \bar{\rho}\widetilde{u}_j\widetilde{\xi^2}}{\partial x_j} = \frac{\partial}{\partial x_j}\Big(\bar{\rho}(\widetilde{D} + D_T)\frac{\partial\widetilde{\xi^2}}{\partial x_j}\Big) - 2\bar{\rho}\widetilde{\chi}_\xi, \quad (5)$$

$$\bar{\rho} = \bar{\rho}(\tilde{\xi}, \widetilde{\xi^2}), \quad \widetilde{T} = \widetilde{T}(\tilde{\xi}, \widetilde{\xi^2}), \quad \bar{\mu} = \bar{\mu}(\widetilde{T}), \quad \widetilde{D} = \widetilde{D}(\widetilde{T}), (6)$$

with $\widetilde{S}_{ij}$ and $\widetilde{\chi}_\xi$ are being the resolved strain rate and scalar dissipation rate, respectively. In the LES momentum equation, Eq.(3), the Smagorinsky model is used to obtain the deviatoric part of the unclosed SGS stress $\tau_{ij} = \bar{\rho}\widetilde{u_iu_j} - \bar{\rho}\widetilde{u}_i\widetilde{u}_j$:

$$\tau_{ij} - \frac{\delta_{ij}}{3}\tau_{kk} = 2\mu_T\Big(\widetilde{S}_{ij} - \frac{\delta_{ij}}{3}\widetilde{S}_{kk}\Big), \quad (7)$$
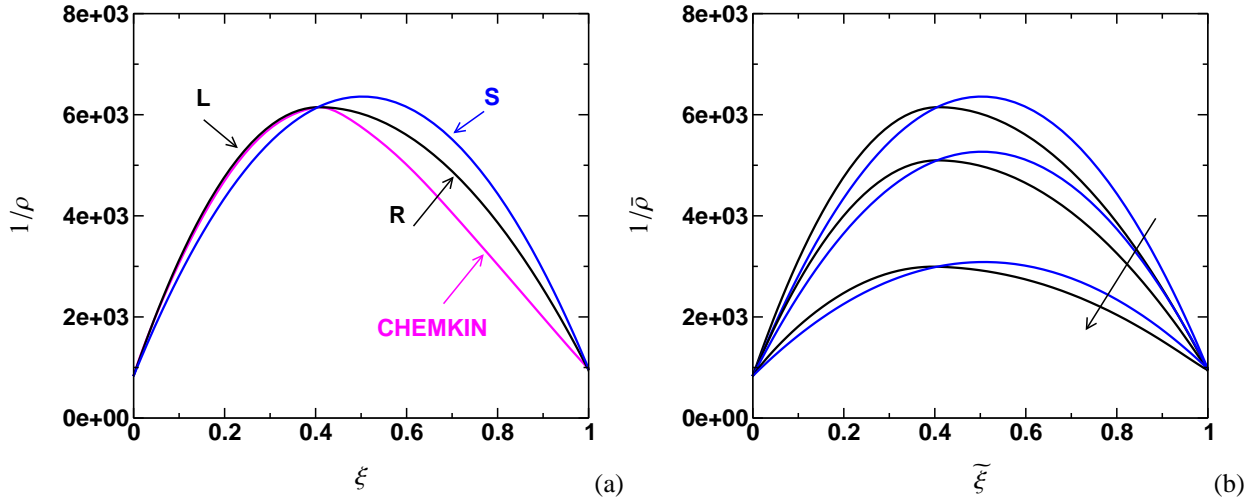
Figure 1: Specific volume vs. mixture fraction: (a) quadratic (S) and piece-wise quadratic (L, R) models compared to the flamelet solution from CHEMKIN; (b) quadratic and piece-wise quadratic models for different values of the subgrid variance $V_\xi = \alpha \widetilde{\xi}(1 - \widetilde{\xi})$ with $\alpha = 0, 0.2, 0.6$ (in descending order).

with the eddy viscosity being $\mu_T = \rho C_S \Delta^2 \sqrt{2\widetilde{S}_{ij}\widetilde{S}_{ij}}$, where the Smagorinsky constant C_S is computed according to Germano dynamic procedure. In both scalar equations, Eqs. (4) and (5), the unclosed subgrid scalar flux is modeled by a standard gradient diffusion hypothesis with the same subgrid diffusivity $\bar{\rho}D_T$ for both scalar fields, for example for the mixture fraction one has:

$$\bar{\rho}\widetilde{u_i\xi} - \bar{\rho}\widetilde{u_i}\widetilde{\xi} = \bar{\rho}D_T \frac{\partial \widetilde{\xi}}{\partial x_i}. \tag{8}$$

The subgrid diffusivity is specified based on the eddy viscosity and the subgrid Schmidt number as $\bar{\rho}D_T = \mu_T/Sc_T$ with a commonly used value of $Sc_T = 0.4$ [11]. Finally, the scalar dissipation rate in Eq. (5) is represented as:

$$\bar{\rho}\widetilde{\chi_\xi} = \overline{\rho D |\nabla \xi|^2} = \bar{\rho}\frac{(D + D_T)}{\Delta^2}(\widetilde{\xi^2} - \widetilde{\xi}^2). \tag{9}$$

A combustion model and transport properties given by Eqs. (1) and (6) are obtained from a steady laminar flamelet solution with the detailed GRI-Mech 3.0 chemical mechanism. A mildly-strained flamelet solution with a strain rate of $a = 130$ s^{-1} is computed in a 1D counter-flow configuration by the OPPDIF module of CHEMKIN 4.1. Unknown density and temperature coefficients are found by fitting a single parabola to the flamelet solution as shown, for the case of density, in Fig. 1(a). It exhibits an adequate approximation for lean mixtures while slightly underpredicting the density for rich mixtures. With the purpose of improving the flamelet approximation we also consider a piecewise quadratic relationship given by:

$$\rho^{-1}(\xi) = \begin{cases} a_L + b_L\xi + c_L\xi^2 & \text{if } \xi < \xi_{max} \\ a_R + b_R\xi + c_R\xi^2 & \text{if } \xi \geq \xi_{max}. \end{cases} \tag{10}$$

In this case the flamelet solution is approximated by the left (L) and the right (R) pieces of parabolas smoothly merging at the maximum point ξ_{max} as shown in Fig. 1(a). These approximations produce a set of nine coefficients a, b, c and $a_{L,R}$, $b_{L,R}$, $c_{L,R}$, respectively, for both density and temperature.

The direct application of the piecewise quadratic approximation to calculate an LES density field, i.e., when subgrid fluctuations are present and the subgrid variance is non-zero, would result in a discontinuity at the maximum point due to differences in the coefficients describing the left and the right branches of a quadratic function. Therefore, to guarantee continuity and smoothness of the resolved density and temperature fields for the whole range of the mixture fraction variance, we assume that the resolved LES fields in the piecewise quadratic representation evolve proportionally to corresponding changes in the approximation described by a single parabola. This translates to the following definition of the resolved density $\bar{\rho}^{-1}(\widetilde{\xi}, \widetilde{\xi^2}) = \widetilde{v}(\widetilde{\xi}, \widetilde{\xi^2})$ (and similarly for temperature):

$$\widetilde{v}(\widetilde{\xi}, \widetilde{\xi^2}) = \left(a_{L,R} + b_{L,R}\widetilde{\xi} + c_{L,R}\widetilde{\xi\xi}\right)\frac{a + b\widetilde{\xi} + c\widetilde{\xi^2}}{a + b\widetilde{\xi} + c\widetilde{\xi\xi}}. \tag{11}$$

This equation easily follows by considering $\widetilde{v}(\widetilde{\xi}, 0) = a_{L,R} + b_{L,R}\widetilde{\xi} + c_{L,R}\widetilde{\xi\xi}$, and the fractional change given by:

$$\frac{\widetilde{v}(\widetilde{\xi}, \widetilde{\xi^2})}{\widetilde{v}(\widetilde{\xi}, 0)} = \frac{a + b\widetilde{\xi} + c\widetilde{\xi^2}}{a + b\widetilde{\xi} + c\widetilde{\xi\xi}}, \tag{12}$$

so that $\widetilde{v}(\widetilde{\xi}, 0)$ is based on the piece-wise quadratic representation, whereas the fractional change on the right hand side due to V_ξ is based on the quadratic representation. Equation (11) is depicted in Fig. 1(b) for several different values
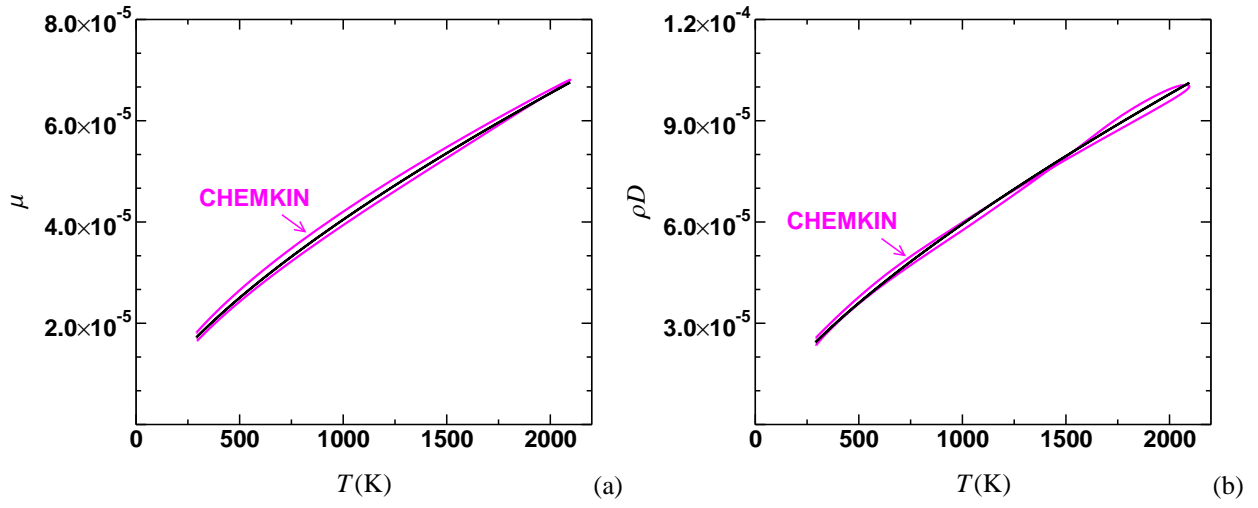
3

Figure 2: Molecular viscosity (a) and diffusivity (b) approximations of CHEMKIN data.
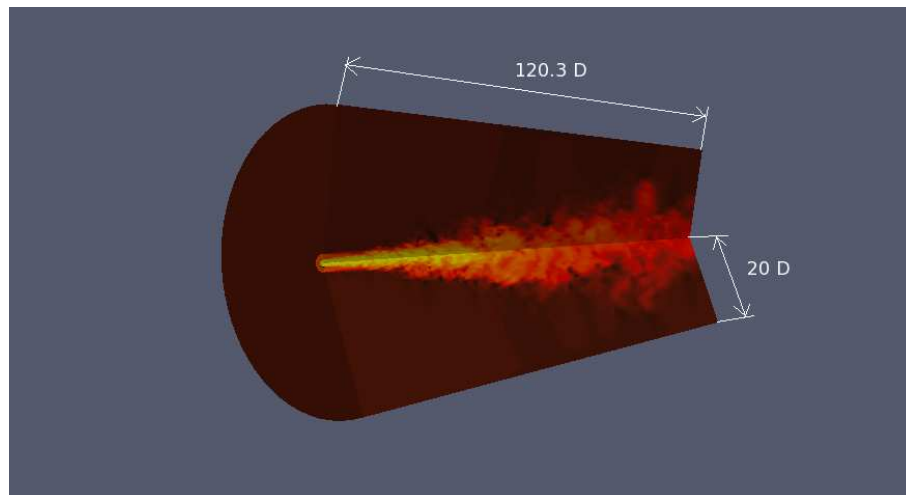

Figure 3: Computational domain and geometrical configuration of Sandia flame D

of the variance and shows continuity while retaining asymmetry with respect to lean and rich parts of the mixture.

The functional dependence of the mixture molecular viscosity and diffusivity on temperature are shown in Fig. 2(a, b). They are computed from CHEMKIN and its thermal and transport databases, and then cast in a power-law form given by:

$$\mu(T) = 1.75 \times 10^{-5} \left(\frac{T}{T_0}\right)^{0.69} \frac{\text{kg}}{\text{m} \cdot \text{s}}, \qquad (13)$$

$$\rho D(T) = 2.48 \times 10^{-5} \left(\frac{T}{T_0}\right)^{0.72} \frac{\text{kg}}{\text{m} \cdot \text{s}}, \qquad (14)$$

with $T_0 = 298$ K. Note that the molecular properties extracted from the flame calculation are double-valued functions of T – with one value on the lean side and one on the rich side of the peak temperature. However, these properties are adequately approximated by the single-valued power laws, Eqs. (13) and (14).

We apply LES Eqs. (2-6) to simulate Sandia flame D that is shown schematically in Fig. 3, and which has been studied experimentally, as fully detailed in [17]. The fuel jet consists of 25% methane/75% air mixture and emanates from a nozzle with diameter $D = 7.2$ mm at a bulk velocity of 49.6 m/s, which defines a characteristic Reynolds number of $Re = 22,400$. The nozzle is surrounded by a coaxial pilot nozzle with diameter of 2.62D. The pilot flow is a lean burnt mixture of C_2H_2, air, CO_2, H_2 and N_2 corresponding to a mixture fraction value of $\xi = 0.271$, with a bulk velocity of 11.4 m/s. The coaxial burner is further surrounded by co-flowing air with a bulk velocity of 0.9 m/s.

In this work the modeled flow configuration is studied in a cylindrical computational domain of $120.3D \times 20D \times 2\pi$ that is represented in cylindrical coordinates (x, r, θ) as depicted in Fig. 3. In the simulations the jet and pilot nozzles have a small axial extension of $0.3D$ upstream of the nozzle exit plane, which is taken as the origin of the axial coordinate, x. The dimensions of the computational domain as well as flow variables are non-dimensionalized by the characteristic jet parameters (i.e., diameter, bulk velocity, density). The turbulent jet inflow velocity condition is generated separately by running a high resolution LES of the stationary turbulent pipe flow enforcing the experimental mean and RMS of axial velocity as measured by the TU Darmstadt group [18]. The turbulent pipe flow simulation has been conducted on a $192 \times 96 \times 96$ grid with periodic boundary conditions in streamwise direction. Inflow velocity conditions for other inflow zones (pilot and co-flow regions) as well as inflow conditions for scalar fields are prescribed based on the corresponding bulk values. Finally, the convective boundary conditions are employed for velocity and scalar fields on the outflow boundary including the entrainment boundary of the computational domain. A structured Stanford LES code is employed to solve the variable-density LES equations, Eqs.

(2-6), written in cylindrical coordinates [23]. The numerical method is second-order accurate in space and time and adopts an energy-conserving discretization scheme for the momentum equation. Scalar transport equations are discretized using the QUICK scheme [28] and solved employing a semi-implicit iterative technique, which has proven to be effective for typical low-Mach combustion problems [23, 29]. Domain decomposition is used for the LES code parallelization.

It is clear from Eqs. (2-6) that the LES solution is a function of the turbulent resolution scale $\Delta(\boldsymbol{x})$. As it is customarily done in practice, we also associate the turbulent resolution scale with the local numerical grid resolution $h(\boldsymbol{x})$, thus enforcing $h(\boldsymbol{x})/\Delta(\boldsymbol{x}) = 1$. In this work we employ five grids $G1, \ldots, G5$ with a progressively increasing resolution from about 0.2 to 10.5 million cells as detailed in Table 1. All grids are stretched in the axial direction as well as in the radial direction, with clustering in the jet nozzle and pilot annulus regions, while remaining uniformly spaced in the circumferential direction. Grid resolution parameters for the jet nozzle and the pilot are given in Table 2.

In all simulations, with an exception of the finest grid $G5$, a zero state is employed as the initial condition for all scalar variables except the velocity field, which is taken to be a uniform and equal to the co-flow velocity in the whole domain. For the finest grid, the initial fields are interpolated from a statistically stationary solution on the preceding grid $G4$. Time integration is performed with a variable time step corresponding to a CFL number of 0.3-0.4. Statistics are accumulated after the simulation has reached a statistically stationary state which is verified by convergence in the RMS statistics. This corresponds to about 12 flow-through times based on the jet bulk velocity and the length of the computational domain. After that the simulation is continued for approximately ten flow-through times. LES statistics $Q^m(\Delta)$ are computed by averaging in time and the circumferential direction, and thus, are functions of x and r. The specific objective of the current work is to study influence of $\Delta(\boldsymbol{x})$ on statistics of the resolved mixture fraction and velocity fields.

Results and Discussion

Before proceeding with the discussion of results, we point out that a complete procedure for the estimation of LES statistics Q^m should include a component which models statistics of the unresolved (residual) motions [25]. In other words, Q^m can be decomposed as $Q^m = Q^W + Q^R$, where Q^W is defined solely by the resolved LES fields, while Q^R estimates the contribution from the residual fields. In this work, we mainly focus on statistics of the resolved fields only, and thus make the approximation $Q^m \approx Q^W$. The modeling of the residual component Q^R will be addressed in future efforts.

Axial profiles of the mean centerline mixture fraction and streamwise velocity are shown in Fig. 4. The veloc-

Grid	Resolution (x, r, θ)	Cells $\times 10^6$	$\Delta^x_{\mathrm{min, max}}$	$\Delta^r_{\mathrm{min, max}}$
G1	$96 \times 64 \times 32$	0.196	$12. \times 10^{-2}, 4.78$	$2.8 \times 10^{-2}, 1.96$
G2	$160 \times 96 \times 64$	0.983	$7.3 \times 10^{-2}, 2.89$	$1.8 \times 10^{-2}, 1.33$
G3	$256 \times 128 \times 64$	2.097	$4.5 \times 10^{-2}, 1.81$	$1.4 \times 10^{-2}, 1.01$
G4	$256 \times 192 \times 96$	4.719	$4.5 \times 10^{-2}, 1.81$	$9.4 \times 10^{-3}, 0.67$
G5	$320 \times 256 \times 128$	10.485	$3.6 \times 10^{-2}, 1.45$	$7.0 \times 10^{-3}, 0.51$

Table 1: Grid parameters and the minimum/ maximum cell width in the axial and radial directions.

Grid	Cells in x for $x < 0$	Cells in r for jet nozzle	Cells in r for pilot	Cells in jet nozzle wall	Cells in pilot wall
G1	3	10	15	2	2
G2	5	15	22	3	3
G3	8	20	30	3	4
G4	8	30	45	4	6
G5	9	40	50	5	7

Table 2: Grid resolutions for the jet nozzle and the pilot.
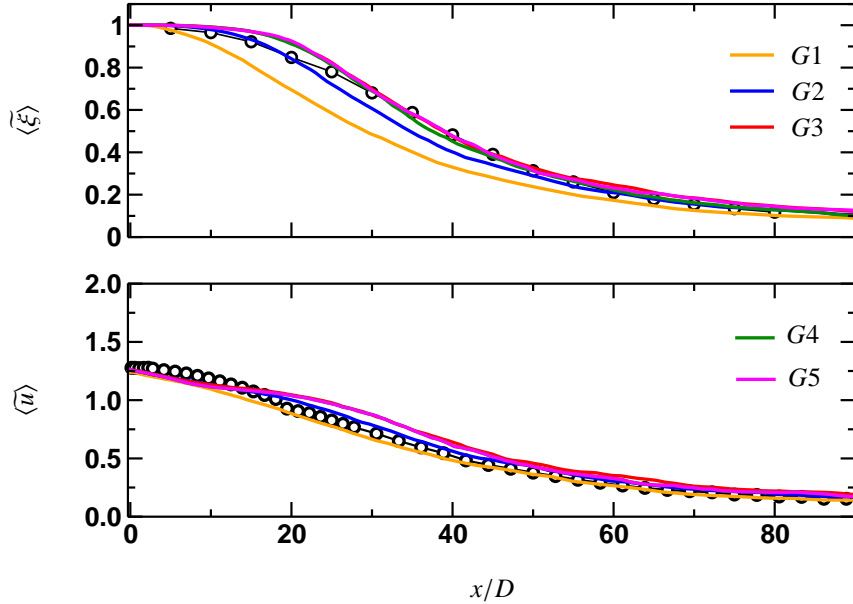
Figure 4: Axial profiles of the centerline mean mixture fraction (top) and mean streamwise velocity (bottom) for different grid resolutions compared with experimental data (symbols). Note that profiles for $G3$, $G4$, $G5$ grids are essentially coincident.
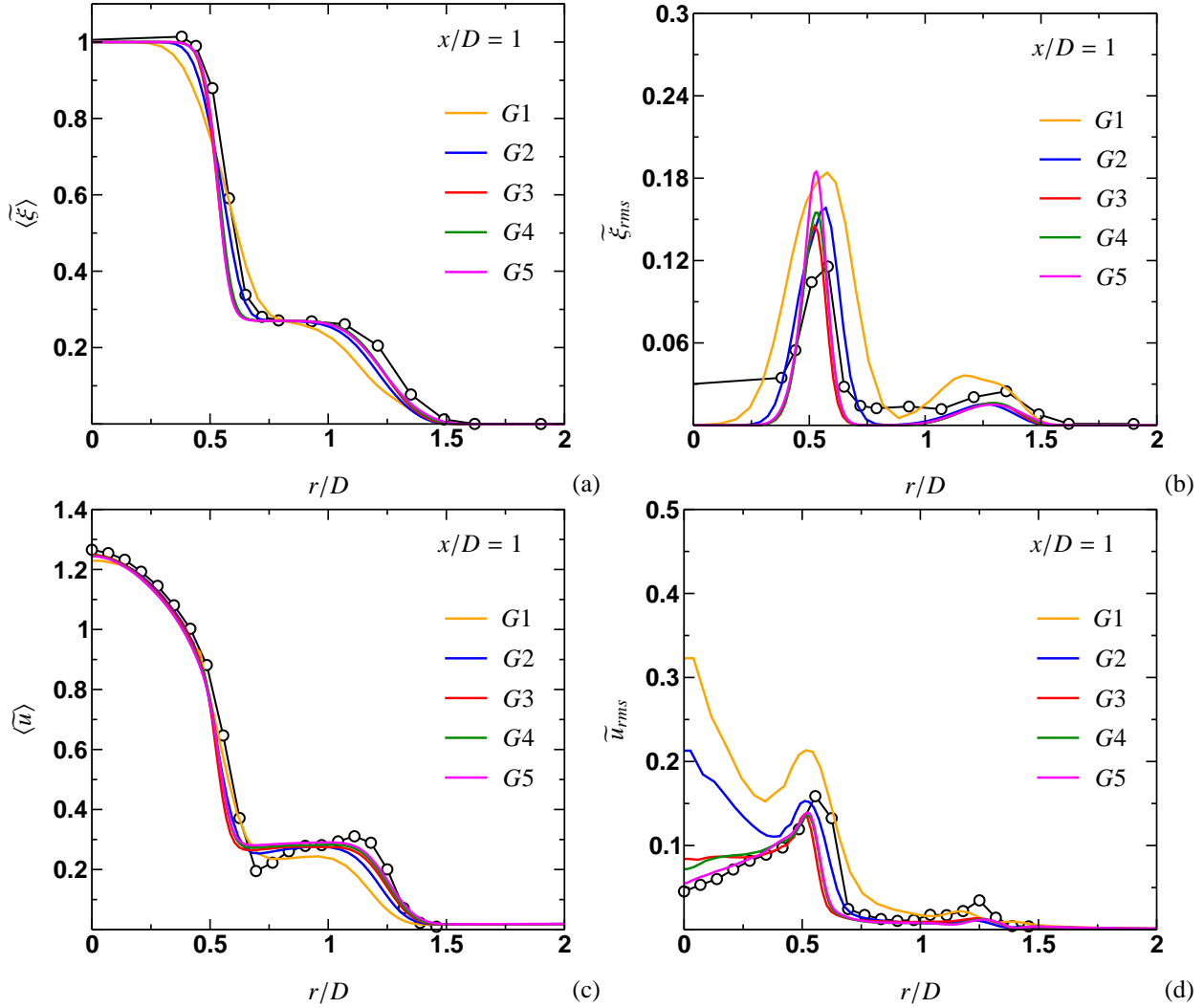
6

Figure 5: Radial profiles of mean and RMS of mixture fraction (a, b) and streamwise velocity (c, d) at the axial location of $x/D = 1$ compared with the experimental data (symbols).
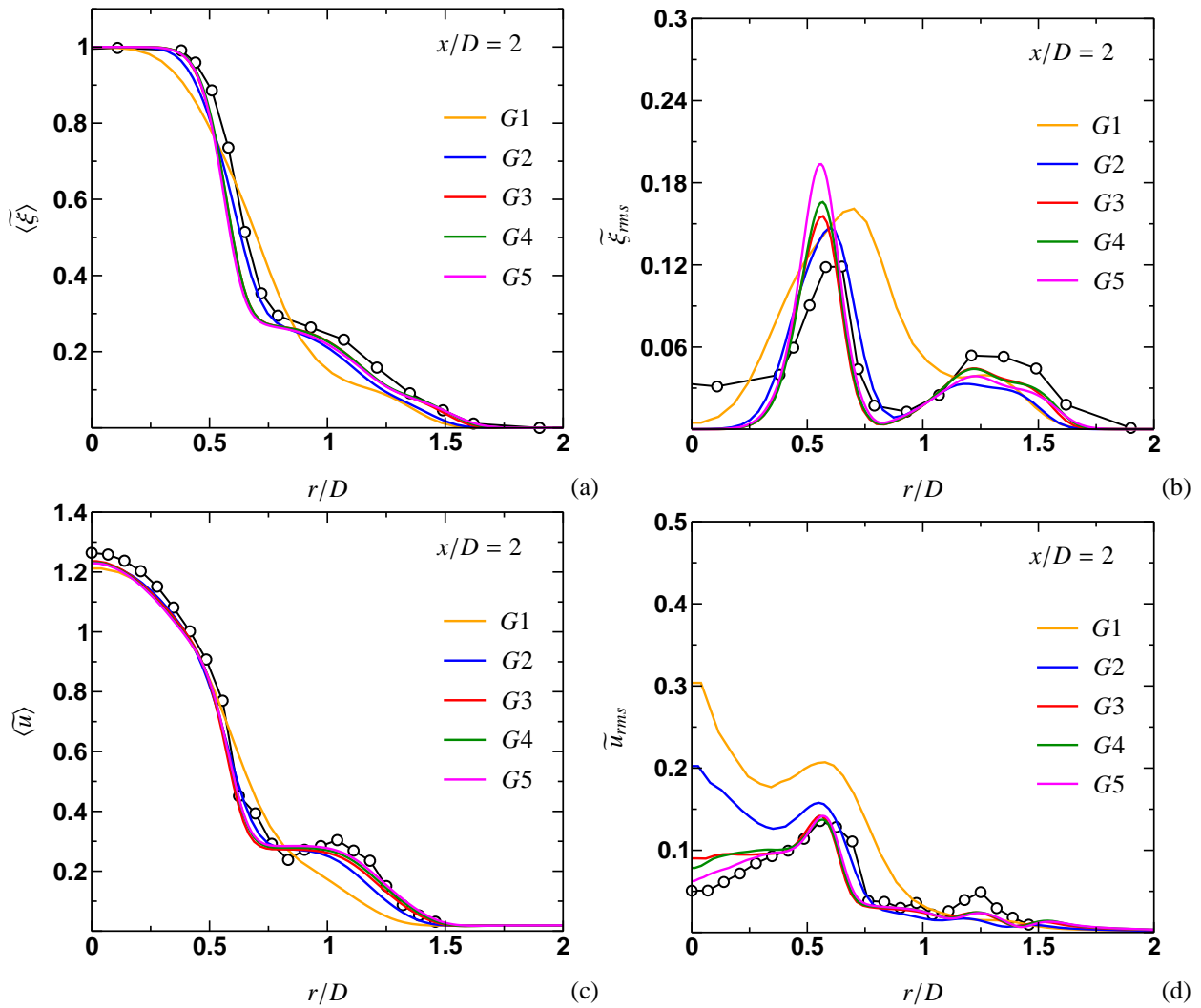
Figure 6: Radial profiles of mean and RMS of mixture fraction (a, b) and streamwise velocity (c, d) at the axial location of $x/D = 2$ compared to the experimental data (symbols).
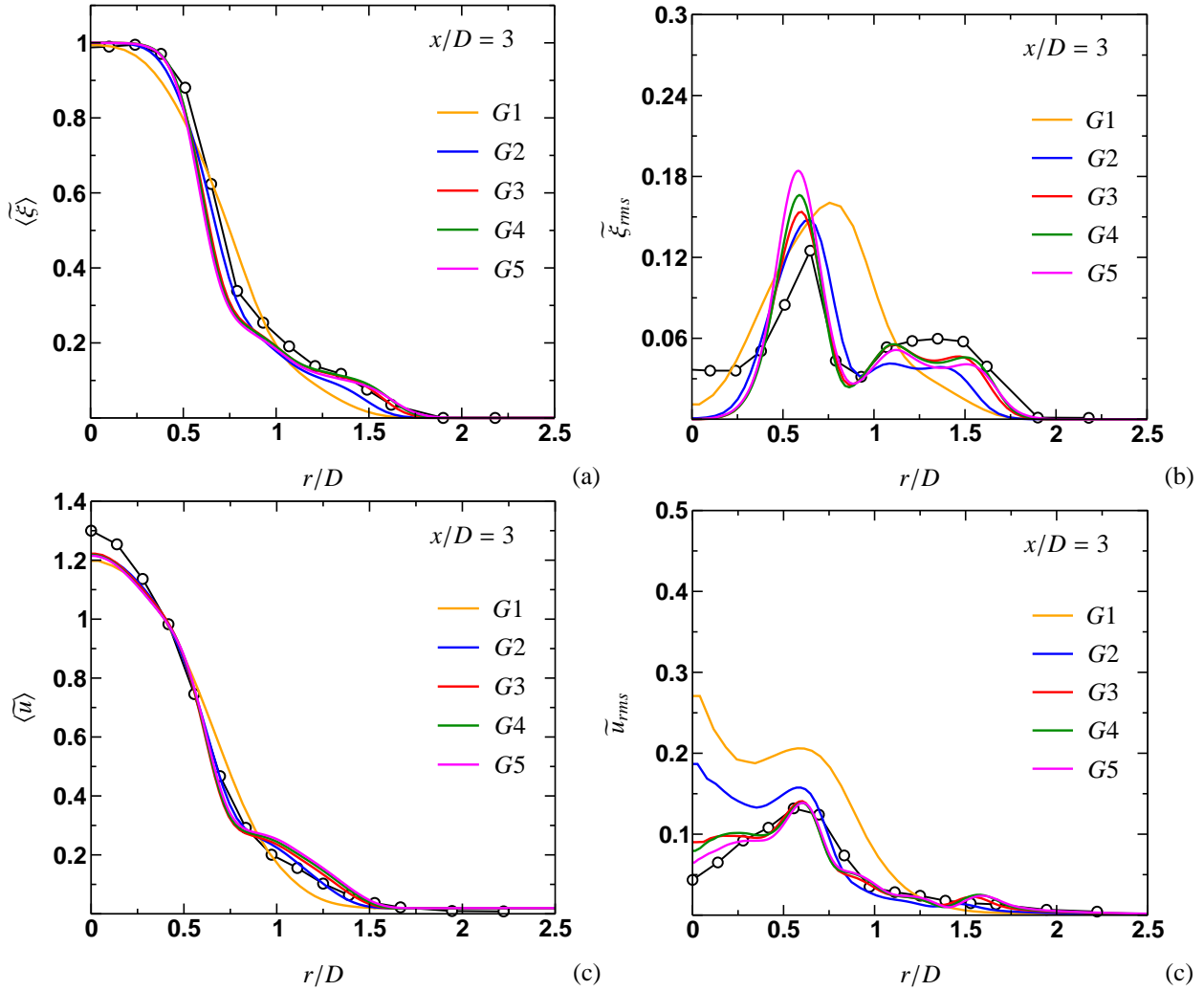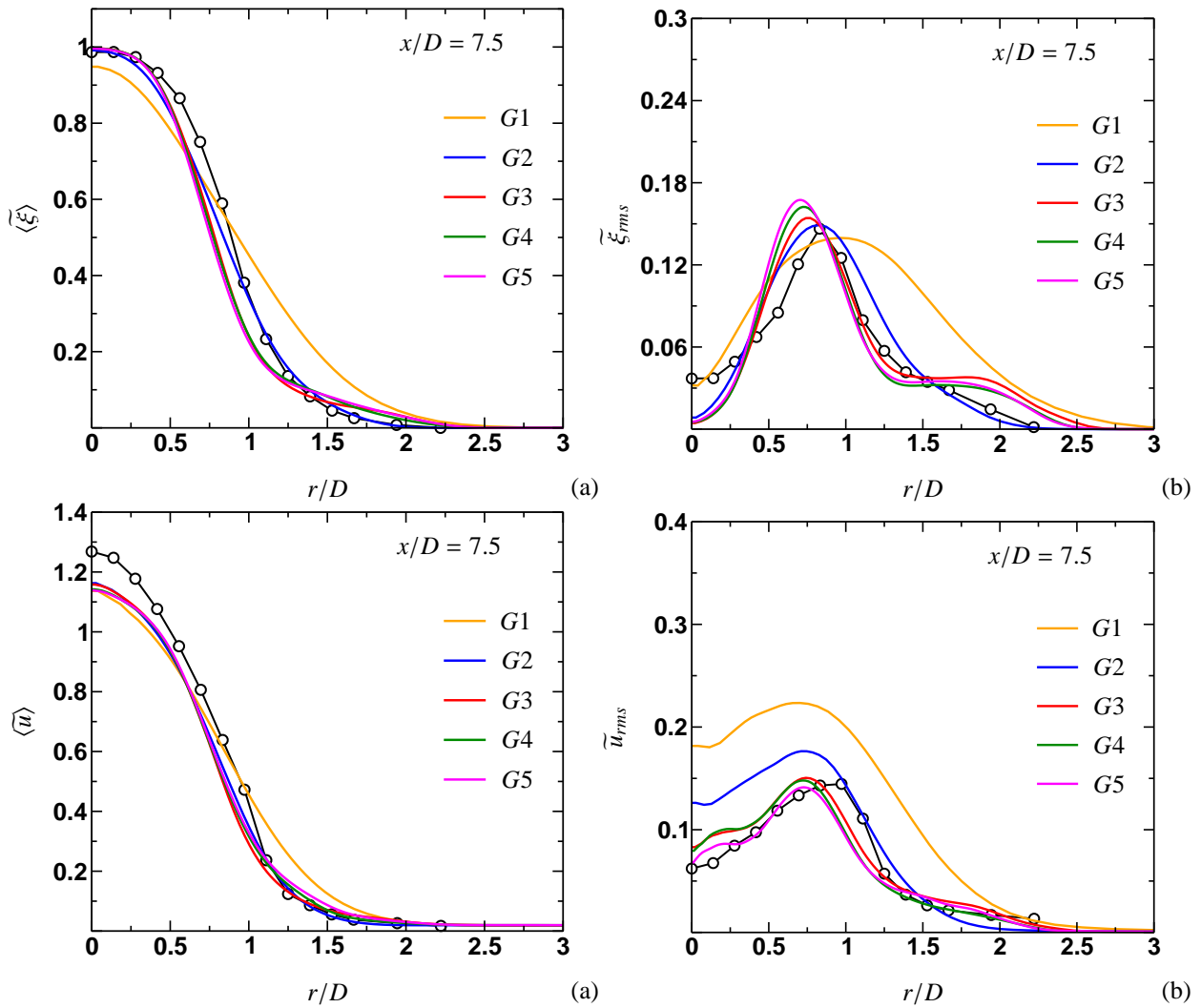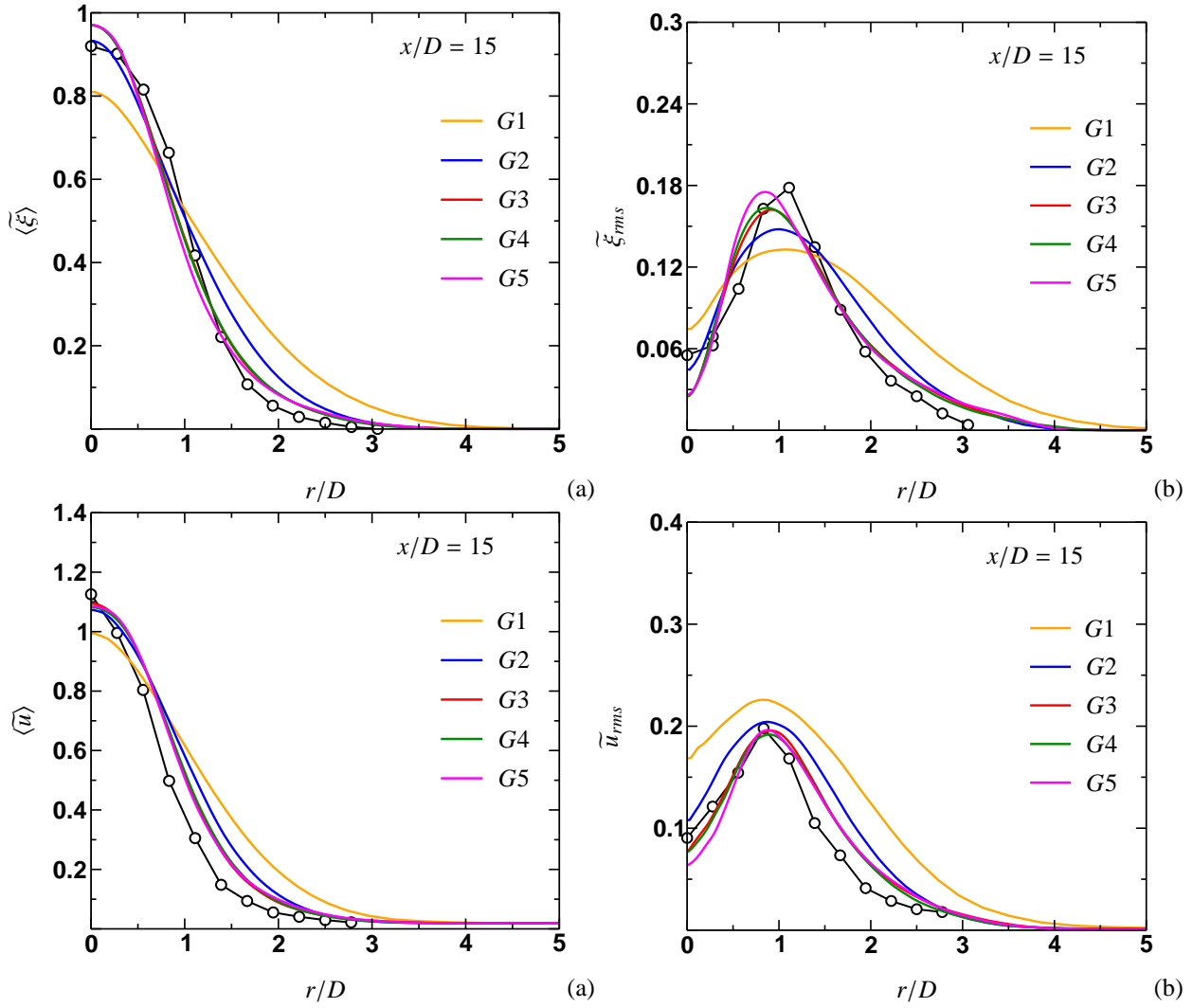
Figure 7: Radial profiles of mean and RMS of mixture fraction (a, b) and streamwise velocity (c, d) at the axial location of $x/D = 3$ compared to the experimental data (symbols).

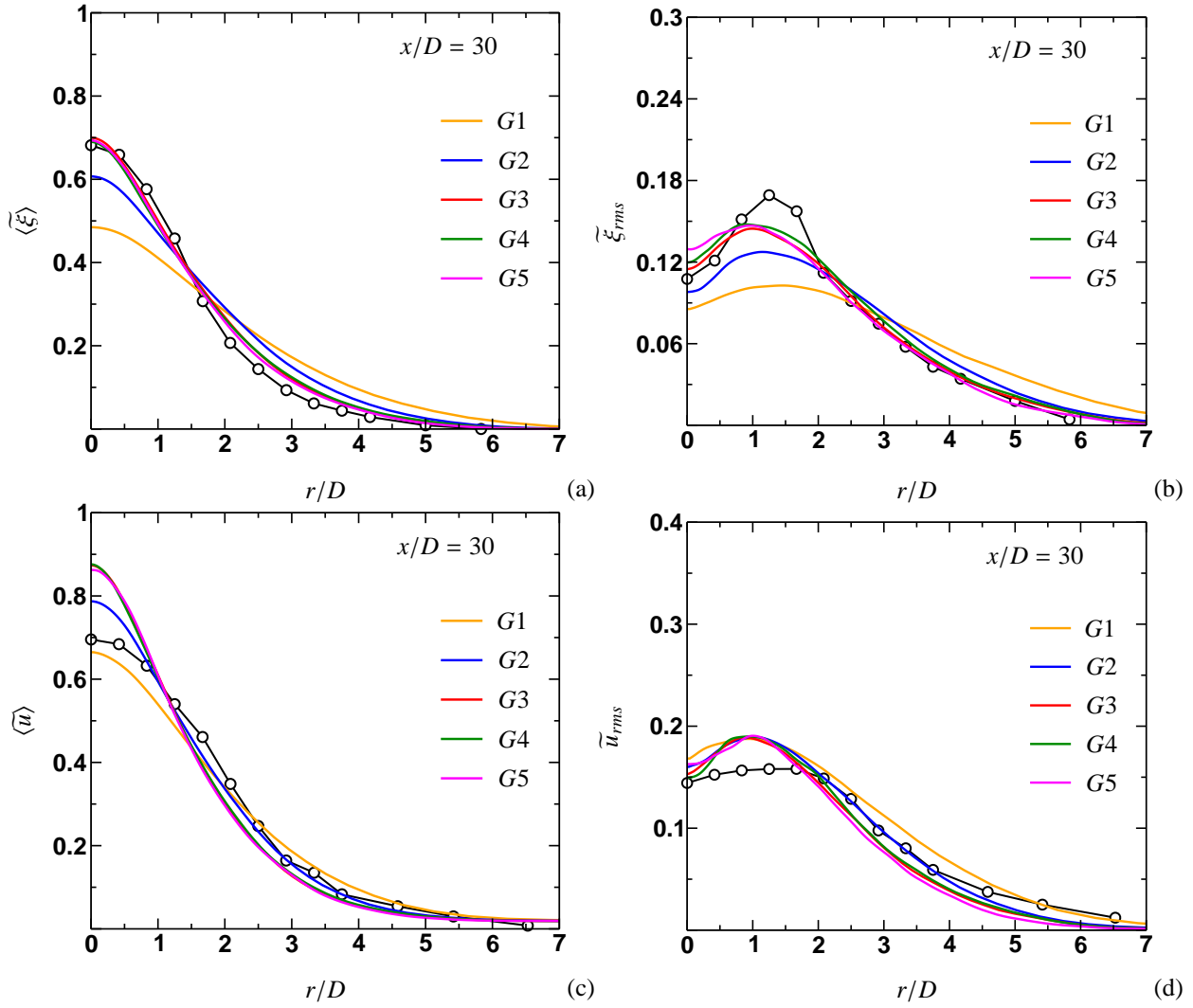Figure 8: Radial profiles of mean and RMS of mixture fraction (a, b) and streamwise velocity (c, d) at the axial location of $x/D = 7.5$ compared to the experimental data (symbols).

Figure 9: Radial profiles of mean and RMS of mixture fraction (a, b) and streamwise velocity (c, d) at the axial location of $x/D = 15$ compared to the experimental data (symbols).

Figure 10: Radial profiles of mean and RMS of mixture fraction (a, b) and streamwise velocity (c, d) at the axial location of $x/D = 30$ compared to the experimental data (symbols).
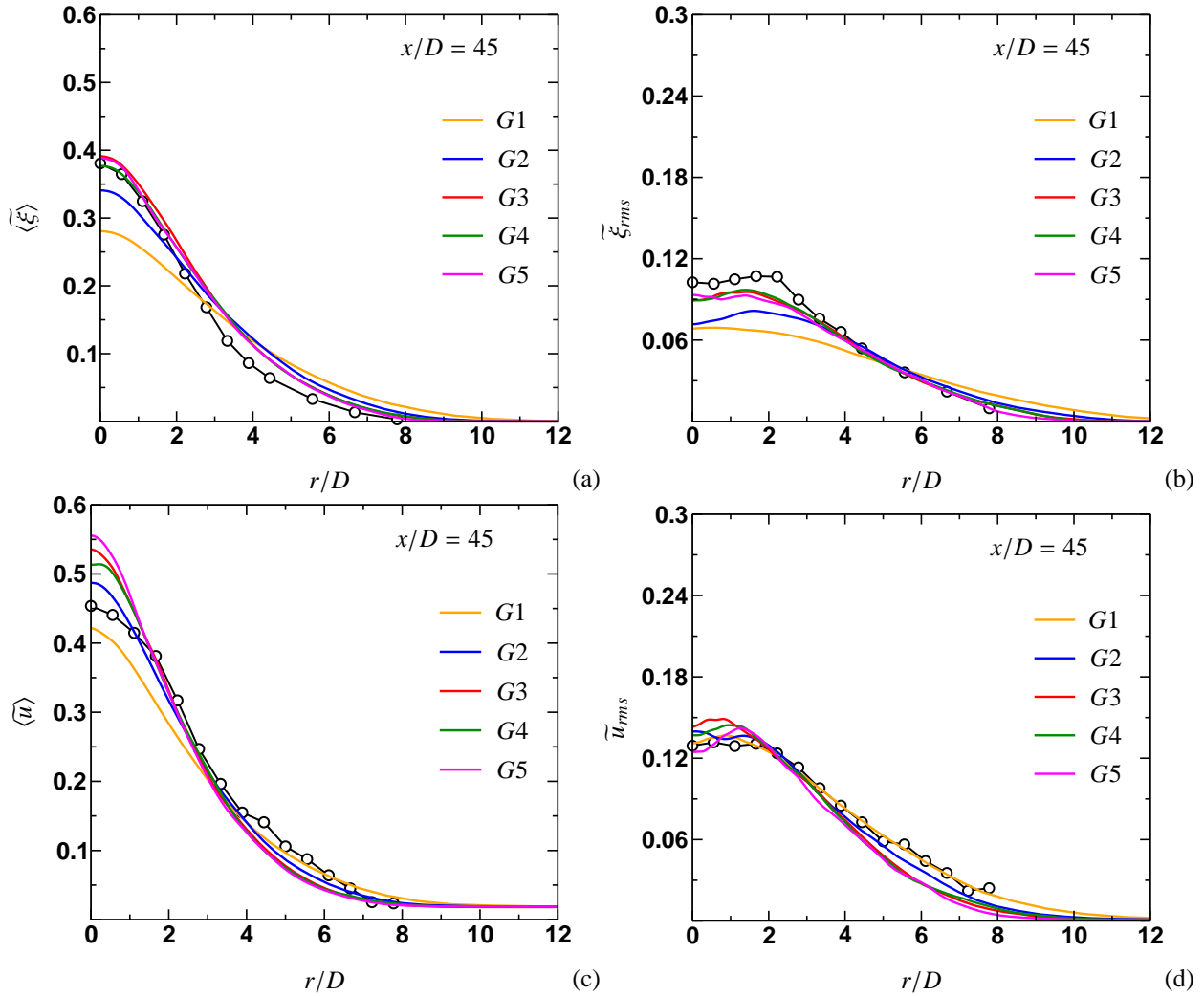
Figure 11: Radial profiles of mean and RMS of mixture fraction (a, b) and streamwise velocity (c, d) at the axial location of $x/D = 45$ compared to the experimental data (symbols).
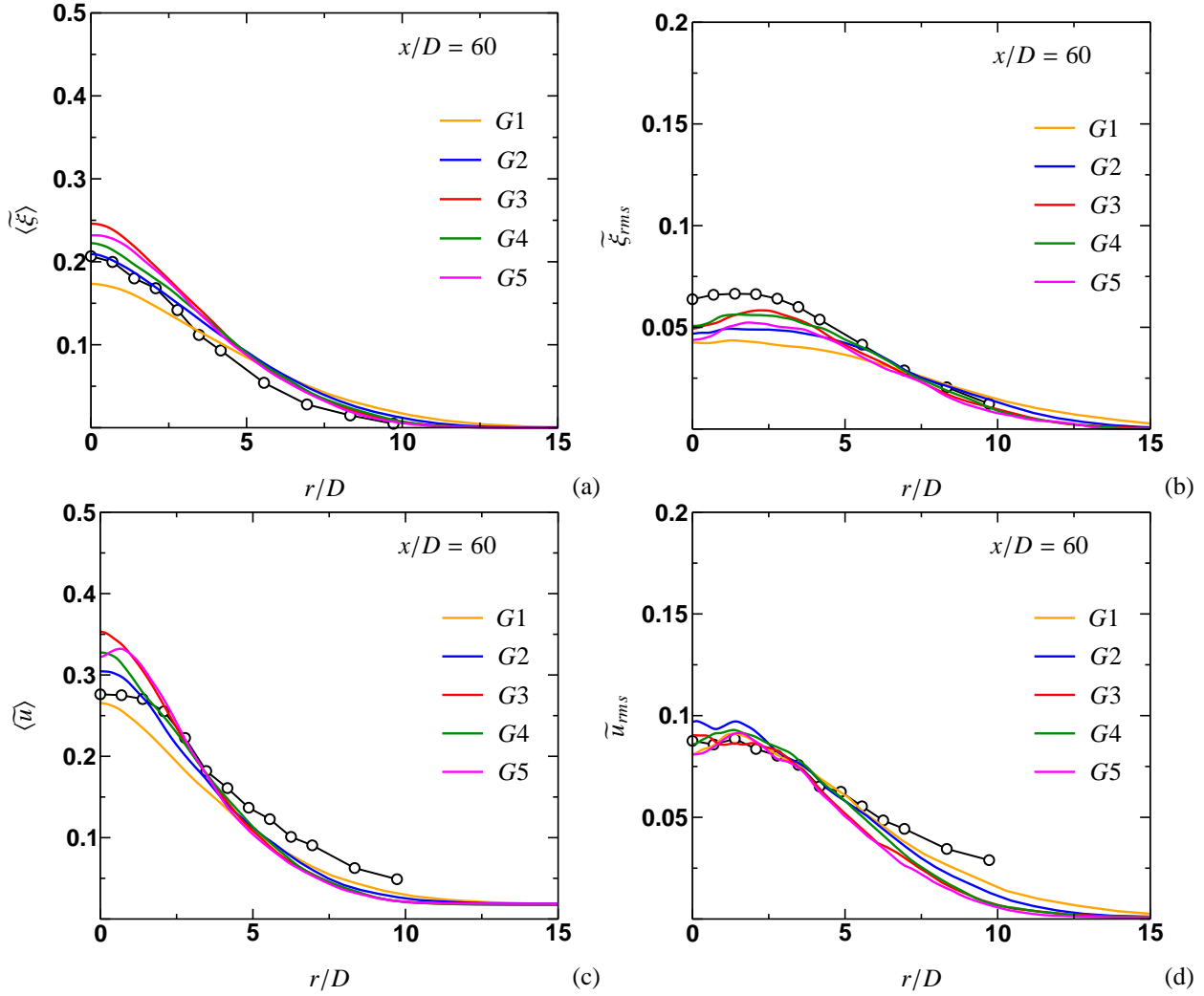
Figure 12: Radial profiles of mean and RMS of mixture fraction (a, b) and streamwise velocity (c, d) at the axial location of $x/D = 60$ compared to the experimental data (symbols).
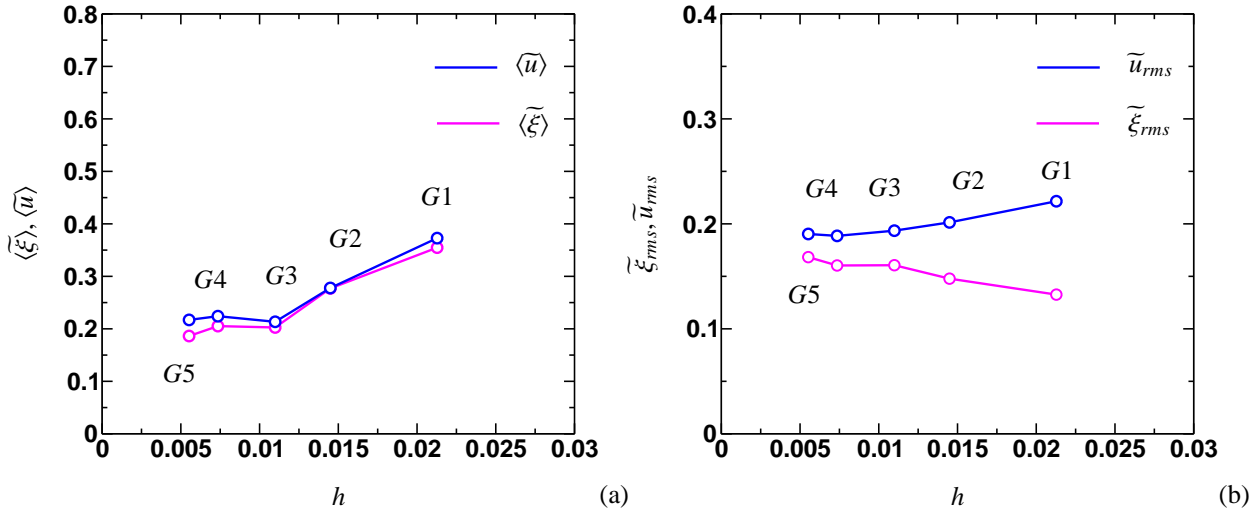
Figure 13: Grid dependence of the mean (a) and the RMS (b) of the streamwise velocity and the mixture fraction at $r/D = 1.5$ and $r/D = 1$, respectively, for a case of $x/D = 15$.

ities shown in these figures are normalized by the jet bulk velocity. Both mean fields exhibit convergence to almost the same asymptotic state starting with the $G3$ grid, while slightly overpredicting the mixture fraction around an axial location of $x/D = 20$. This delay of mixing is consistent with the adopted quadratic model for which temperature values are overpredicted for rich mixtures (with a maximum overprediction of 20% around $\xi = 0.7 - 0.8$). The coarser grid $G2$, on the other hand, provides a better estimation of the mean mixture fraction at this location with some underprediction further downstream, which can be attributed to an excessive fluctuating contribution from the dynamically computed eddy viscosity and diffusivity. It is interesting to note that the coarsest grid $G1$ gives a quite reasonable prediction of the mean velocity, measured at TU Darmstadt [18], where the mean mixture fraction is substantially below the experimental level measured at Sandia [17].

Figures 5-12 exhibit radial profiles of the corresponding mean and RMS quantities at different axial locations. It can be seen that, on the $G1$ and $G2$ grids, the resolved streamwise velocity in the near field (up to $x/D = 7.5$) is characterized by excessive fluctuations, especially on the centerline. This is probably caused by an underresolution in the radial direction in the explicitly simulated jet nozzle, as further evident comparing Figs. 5(c)-8(c). The radial resolution in the jet pipe is 10 and 15 cells for $G1$ and $G2$, and 20, 30, 40 cells, respectively, for grids $G3$, $G4$, $G5$. As a result, excessive centerline velocity fluctuations penetrates the near field but decay quickly after $x/D = 7.5$.

Figures 5-9 show that the mixture fraction and velocity reach an intermediate asymptotic stage for the resolution scale finer than that of $G2$. This also characterizes both velocity RMS fields and the mixture fraction RMS fields,

the latter, however, shows a little more complicated behavior. As can be seen from Figs. 5(b)-9(b), the mixture fraction RMS profiles exhibit a visible sensitivity to the turbulent resolution scale Δ at the locations of their maxima ($r/D \sim 0.5 - 1.0$), i.e., in a mixing layer between jet fuel and hot pilot products. A less pronounced sensitivity is also seen in the mixing layer between pilot product and co-flow air at the initial stage, but it is weaker and disappears at a location of $x/D = 15$. Such a behavior suggests that the adopted LES model, while performing adequately in most of the domain, is not able to capture the small-scale scalar processes in the high-gradient regions. Further downstream, as the scalar gradient decreases, the mixture fraction RMS shows less sensitivity to Δ and reaches an approximate asymptotic stage.

The dependence of LES statistics on the resolution scale is further highlighted in Figs. 13(a, b). Here, the mean and RMS values of the mixture fraction and streamwise velocity are plotted versus the grid spacing measure h. These profiles correspond to radial locations of $r/D = 1.5$ for the mean, and $r/D = 1.0$ for the RMS, respectively, and for an axial location of $x/D = 15$ (compare to Fig. 9). Since all grids are non-uniform, the grid spacing measure h is defined as the inverse of the number of cells in the jet (in the radial direction). It is seen that the velocity statistics attain its approximate asymptotic state, while the mixture fraction statistics exhibit a discernible change between the two finest grids, $G4$ and $G5$.

It can be further noted that at the far field locations the mean streamwise velocity (at $x/D = 45$ and $x/D = 60$) and mixture fraction (at $x/D = 60$) start deviating from the intermediate asymptotic stage in a vicinity of the centerline as shown in Figs. 11, 12. The reason for this could be two-fold: first, the far field locations clearly require longer

runs to accumulate an equivalent statistically representative ensemble (compared to near-field locations); second, the increase in cell size due to stretching in the axial direction may be excessive. Finally, we note that the coarsest $G1$ grid provides the best approximation for RMS of the streamwise velocity at $x/D = 45$ (Fig. 11(d)) as well as a reasonably good approximation for the mean of the streamwise velocity on the centerline (Fig. 4), which does not make this LES solution satisfactory. Thus, it is important to consider the dependence of an LES solution on $\Delta(\boldsymbol{x})$, and to have a procedure to specify it optimally.

Conclusions

LES of the piloted non-premixed Sandia flame D have been performed on a series of grids with progressively increasing resolution from 0.19 to 10.4 million cells, with the purpose of studying the sensitivity of LES statistics to the turbulence resolution scale $\Delta(\boldsymbol{x})$.

In the present effort, a simple combustion model has been adopted to parametrize reacting density and temperature in terms of the mixture fraction and its square (or subgrid variance). As a result, two transport equations for these scalars need to be integrated. Coefficients for quadratic analytic approximations of specific volume and temperature have been obtained based on a flamelet CHEMKIN simulation with a detailed chemistry mechanism. These approximations are found to be quite accurate for lean mixtures while slightly underpredicting the reacting density for rich ones. In addition, the smoothness of the quadratic model eliminates the effect of interpolation uncertainties on an LES solution and its statistical dependence on the turbulence resolution scale $\Delta(\boldsymbol{x})$.

Mean and RMS values of the mixture fraction and streamwise velocity have been chosen as representative LES statistics of interest. Generally, a simply combustion model is found to be capable to reproduce essential features of Sandia flame D, especially on fine grids. The hypothesis of the intermediate asymptotic behavior of LES statistics with respect to $\Delta(\boldsymbol{x})$ has been tested and found to hold true throughout the most of the flow domain. However, the RMS of the mixture fraction is found to be non-convergent to an asymptotic state in high scalar gradient regions.

References

[1] J. Janicka, A. Sadiki, Proc. Combust. Inst. 30 (2005) 537–547.

[2] H. Pitsch, Ann. Rev. Fluid Mech. 38 (2006) 453–482.

[3] J. J. Riley, J. Fluids Engrg. 128 (2006) 209–215.

[4] J. C. Oefelein, Prog. Aero. Sci. 42 (2006) 2–37.

[5] S. Menon, P. A. McMurtry, A. K. Kerstein, in: Large Eddy Simulation of Complex and Geophysical Flows, Cambridge University Press, 1993.

[6] W. K. Bushe, H. Steiner, Phys. Fluids 11 (1998) 1896–1906.

[7] S. Navarro-Martinez, A. Kronenburg, F. di Mare, Flow Turb. Combust. 75 (2005) 245–274.

[8] V. Raman, H. Pitsch, R. O. Fox, Combust. Flame 143 (2005) 56–78.

[9] P. Givi, AIAA J. 44 (2006) 16–23.

[10] A. W. Cook, J. J. Riley, Combust. Flame 112 (1998) 593–606.

[11] H. Pitsch, H. Steiner, Phys. Fluids 12 (2000) 2541–2554.

[12] A. Kempf, R. P. Lindstedt, J. Janicka, Combust. Flame 144 (2006) 170–189.

[13] A. W. Vreman, B. A. Albrecht, J. A. van Oijen, L. P. H. de Goey, R. J. M. Bastiaans, Combust. Flame 153 (2008) 394–416.

[14] W.-W. Kim, S. Menon, H. C. Mongia, Combust. Sci. Tech. 143 (1999) 25–62.

[15] F. di Mare, W. P. Jones, K. R. Menzies, Combust. Flame 137 (2004) 278–294.

[16] K. Mahesh, G. Constantinescu, S. Apte, G. Iaccarion, F. Ham, P. Moin, J. Appl. Mech. 73 (2006) 374–381.

[17] R. S. Barlow, J. H. Frank, Proc. Combust. Inst. 27 (1998) 1087–1095.

[18] C. Schneider, A. Dreizler, J. Janicka, E. P. Hassel, Combust. Flame 135 (2003) 185–190.

[19] A. Kempf, F. Flemming, J. Janicka, Proc. Combust. Inst. 30 (2005) 557–565.

[20] V. Raman, H. Pitsch, Proc. Combust. Inst. 31 (2007) 1711–1719.

[21] D. J. Clayton, W. P. Jones, Flow Turb. Combust. 81 (2008) 497–521.

[22] N. Peters, Prog. Energy Combust. Sci. 10 (1984) 319–339.

[23] C. D. Pierce, P. Moin, J. Fluid Mech. 504 (2004) 73–97.

[24] S. B. Pope, Prog. Energy Combust. Sci. 11 (1985) 119–192.

[25] S. B. Pope, New J. Phys. 6 (2004) 35.

[26] T. Hughes, L. Mazzei, K. Jansen, Comput. Vis. Sci. 3 (2000) 47–59.

[27] J.-L. Guermond, J. T. Oden, S. Prudhomme, J. Math. Fluid Mech. 6 (2004) 195–248.

[28] B. P. Leonard, Comput. Methods Appl. Math. Engrg. 19 (1979) 59–98.

[29] V. Raman, H. Pitsch, Combust. Flame 142 (2005) 329–347.